

Enhanced Tumor Targeting of Radiolabeled Mouse/Human Chimeric Anti-Tn Antibody in Losartan-Treated Mice Bearing Tn-Expressing Lung Tumors

Marcos Tassano (✉ tassanom@gmail.com)

Universidad de la República

Ximena Camacho

Universidad de la República

Teresa Freire

Universidad de la República

Carolina Perroni

Universidad de la República

Valeria da Costa

Universidad de la República

Mirel Cabrera

Universidad de la República

Maria Fernanda García

Universidad de la República

Marcelo Fernandez

Universidad de la República

Juan Pablo Gambini

Universidad de la República

Pablo Cabral

Universidad de la República

Eduardo Osinaga

Institut Pasteur de Montevideo

Article

Keywords:

Posted Date: July 18th, 2023

DOI: <https://doi.org/10.21203/rs.3.rs-3139336/v1>

License:  This work is licensed under a Creative Commons Attribution 4.0 International License.

[Read Full License](#)

Abstract

ChiTn, a mouse/human chimeric anti-Tn monoclonal antibody, was radiolabeled with iodine-131 (^{131}I) and technetium-99m ($^{99\text{m}}\text{Tc}$) to assess its biodistribution and internalization in Tn-expressing (Tn+) and wild-type (Tn-) LL/2 lung cancer cells. Selective accumulation and gradual internalization of ChiTn were observed in Tn + cells. Biodistribution in mice with both Tn + or Tn- lung tumors indicated that the uptake of radiolabeled ChiTn within tumors increased over time. Dual-labeling experiments with $^{99\text{m}}\text{Tc}$ and ^{131}I showed different biodistribution patterns, with $^{99\text{m}}\text{Tc}$ exhibiting higher values in the liver, spleen, and kidneys, while ^{131}I showed higher uptake in the thyroid and stomach. However, tumor uptake did not significantly differ between Tn + and Tn- tumors. To improve tumor targeting, Losartan, an antihypertensive drug known to enhance tumor perfusion and drug delivery, was investigated. Biodistribution studies in Losartan-treated mice revealed significantly higher radiolabeled ChiTn uptake in Tn + tumors. No significant changes were observed in the uptake of the control molecule IgG-HYNIC- $^{99\text{m}}\text{Tc}$. These findings demonstrate the enhanced tumor targeting of radiolabeled ChiTn in Losartan-treated mice with Tn-expressing lung tumors. They highlight the potential of ChiTn as a theranostic agent for cancer treatment and emphasize the importance of Losartan as an adjunctive treatment to improve tumor perfusion and drug delivery.

Introduction

Monoclonal antibodies (mAbs) have been widely used in clinical practice for the diagnosis and treatment of various human pathologies, including cancer and infectious diseases, as well as for the modulation of the immune response (Buss et al., 2012; Hafeez et al., 2018; Kaplon & Reichert, 2021). The development of therapeutic mAbs in cancer has been facilitated by the identification of cell surface structures. These structures, which are either present or overly expressed in abnormal cells compared to their normal counterparts, act as targets for the effective function of mAbs (Martineau et al., 2018). Aberrant glycosylation is a common change in cancer cells, which causes incomplete elongation of the carbohydrate chains and unmasking of tumor-associated carbohydrate antigens on the cell surface (Hakomori, 2002). The Tn-antigen (CD175) is formed by an N-acetyl galactosamine (GalNAc) residue O-linked to the amino acids serine or threonine, present in the amino acid sequence of different glycoproteins, especially those of the mucin-type (Ju et al., 2011). This antigen is a cryptic determinant in cancer with high expressions in various epithelial cancers (ovarian, breast, prostate, colorectal, and lung cancers) (Hubert et al., 2011; Sedlik et al., 2016). Tn is associated with metastasis and cancer aggressiveness (Fu et al., 2016; Liu et al., 2019). Indeed, in Lewis lung cancer (LL/2), Tn antigen promotes tumor growth, immune evasion, and angiogenesis, resulting in larger and highly vascularized tumors (da Costa et al., 2021). This may be explained by the ability of LL/2 Tn + cells and LL/2 Tn + tumors to produce higher amounts of vascular endothelial growth factor (VEGF) compared to LL/2 wild type (Tn-) (da Costa et al., 2021). VEGF is considered to be the primary angiogenesis factor and has been shown to play a role in inducing extracellular matrix (ECM) synthesis and the angio-fibrotic switch in fibrosis (Larsson-Callerfelt et al., 2017; Kuiper et al., 2008; Zhang et al., 2019). Fibrosis, characterized by the

excessive deposition of collagen, hyaluronan, and other ECM components, plays a critical role in tumor progression (Zhang et al., 2019). The fibrotic ECM has been identified as a significant contributor to the elevated solid stress observed in tumors (Jain et al., 2014). Unlike fluid pressure, this physical force is specifically contained within and transmitted by the solid phase of the tumor, resulting in the compression of blood vessels. This compression, coupled with the structural abnormalities of tumor blood vessels, renders them highly susceptible to collapse under the influence of the increased compressive forces. Consequently, the overall blood flow throughout the tumor mass is compromised (Liu et al., 2012; Chauhan et al., 2013; Jain et al., 2014; Nia et al., 2016). This reduction in perfusion has two major consequences: (i) compromised efficacy of treatment due to reduced drug delivery to tumors (Stylianopoulos et al., 2018), and (ii) increased tumor hypoxia, which promotes aggressive phenotypes, immunosuppression, and resistance to chemotherapy, radiation, and immunotherapy, all of which require oxygen to be effective (Jain, 2014). Therefore, strategies aimed at reducing solid stress and improving tumor perfusion are being explored as a means to improve the delivery and efficacy of cancer therapeutics. One such strategy is the use of Losartan, an FDA-approved antihypertensive agent that has been shown to improve tumor perfusion and drug delivery in mouse models of breast and pancreatic cancer by reducing the collagen and hyaluronan content within tumors (Diop-Frimpong et al., 2011; Chauhan et al., 2013; Zhao et al., 2019).

Several mAbs targeting the Tn-antigen with different specificities have been developed, some of which have demonstrated increased survival in mice inoculated with Jurkat (Ando et al., 2018), mammary (Hubert et al., 2011), and lung carcinoma cell lines (Wellinder et al., 2011). In addition to their inherent ability to inhibit tumor growth by inducing or stimulating the immune system (Scott et al., 2012; Vacchelli et al., 2013), the antitumor efficacy of mAbs can be significantly enhanced by conjugation with drugs (Chau et al., 2019), oligonucleotides (Dovgan et al., 2019), or radionuclides (Steiner & Neri, 2011; Audicio et al., 2011; Camacho et al., 2017; Perroni et al., 2021). A mouse/human IgG1 chimeric anti-Tn mAb, ChiTn, has been developed and used as an antibody-drug conjugate. Results showed that ChiTn internalizes in Tn + tumor cells *in vitro* and selectively accumulates in the tumor *in vivo* (Sedlik et al. 2016).

Imaging and biodistribution studies utilizing radioactive tracers have emerged as a highly sensitive and versatile approach, making it one of the main approaches for *in vitro* and *in vivo* studies of molecular-level processes. It allows analysis of pharmacokinetics, heterogeneity, antigen expression and engagement, and uptake of radiolabeled mAbs in tumors and other organs (Harsini & Rezaei, 2020; Perroni et al. 2021; Lin et al., 2021). Among commonly used radionuclides in nuclear medicine, iodine-131 (^{131}I) stands out as a dual β and γ emitter with an 8.02-day half-life, being suitable for both tracer studies and therapeutic applications (Zhang et al., 2022). Additionally, technetium-99m ($^{99\text{m}}\text{Tc}$), with its 6-hour half-life and γ -ray emission, provides valuable capabilities for imaging and biodistribution studies (Duatti, 2021).

In this study, we aimed to explore the potential of a radiolabeled mouse/human IgG1 chimeric anti-Tn mAb (ChiTn) as a theranostic agent for cancer. We radiolabeled ChiTn with ^{131}I and $^{99\text{m}}\text{Tc}$, and evaluated

its biodistribution and internalization in Tn + and Tn- (wild-type) cells. Furthermore, we investigated the potential use of Losartan as an adjunctive treatment to enhance the delivery and targeting of radiolabeled ChiTn to Tn + tumors in murine models of Tn + and Tn- LL/2 lung cancer.

Methods

ChiTn and IgG linker formation

The mouse/human IgG1 chimeric anti-Tn mAb (Chi-Tn) (Osinaga et al., 2000) was obtained from Laboratorio de Glicobiología e Inmunología tumoral / Institut Pasteur Montevideo. A human IgG (Sigma-Aldrich, USA) was used as a control molecule, which has no declared antigen-specificity. The conjugation reaction was initiated by adding a N-succinimidyl 6-(trifluoroacetyl) hydrazinopyridine-3-carboxylic acid hydrazino-protected form of succinimidyl ester (NHS-HYNIC-Tfa), synthesized in our laboratory (Garcia et al., 2014), and 100 nmol in 7 μ L dimethylsulfoxide ((DMSO), J. T. Baker) were added to purified ChiTn or IgG control (10 nmol) in, 0.15 M pH 8 $\text{NaC}_2\text{H}_3\text{O}_2$ buffer and incubated in darkness for 30 min at room temperature (RT). The ChiTn-HYNIC and IgG-HYNIC were subsequently purified by size-exclusion chromatography using NaCl 0.9% and a Sephadex G-25 (SEC) column (PD-10, Amersham Biosciences).

ChiTn and IgG radiolabeling

Radiolabeling of ChiTn-HYNIC or IgG-HYNIC with $^{99\text{m}}\text{Tc}$ was performed by adding 33.5 mol of tricine, 33 mol of $\text{SnCl}_2 \cdot 2\text{H}_2\text{O}$, and 5 nmol of the antibody conjugate. Immediately, a $\text{Na}^{99\text{m}}\text{TcO}_4^-$ solution was added, and the mixture was incubated at RT for 30 min. Radiolabeling of ChiTn or IgG with ^{131}I was achieved using the Pierce pre-coated iodination tubes (PPCIT) (Thermo Fisher Scientific, Waltham, MA, USA), and the "Example Protocol I: The Chizzonite Indirect Method for Iodination" protocol according to Thermo Fisher Scientific manual 0016379. Briefly, the PPCIT was wetted with 1 ml of Tris iodination buffer and decanted. Then, 10 MBq of ^{131}I were added to the PPCIT and activated for 6 min at RT. Subsequently, 50 μ g of ChiTn or IgG were added and the reaction mixture was incubated for 10 min at RT.

ChiTn and IgG radiolabeling controls, purification, and stability

Both radiolabeling were evaluated for radiochemical purity by 1) SEC equilibrated and eluted with normal saline, at 1.0 mL/min flow rate, and 2) High-performance liquid chromatography (HPLC) with a Protein-Pak 300 SW 7.5 mm x 30 cm column (Waters, USA) using isocratic mode with 0.05 M pH 7.0 phosphate buffer, 1 mL/min flow rate, equipped with UV and NaI(Tl) absorbance and scintillation detectors respectively. Technetium-99m radiolabeling was assessed using Instant thin-layer chromatography (ITLC) chromatography with various systems: ITLC-SG (Pall Corporation) combined with 0.9% NaCl, ITLC-SG saturated with bovine serum albumin (BSA, Sigma-Aldrich) and EtOH:NH₃:H₂O (2:1:5), as well as Whatman 1 paper (Whatman International Ltd) with methyl ethyl ketone (MEK). To ensure the integrity of the radiolabeled antibodies, the same HPLC system was employed. The radiolabeled antibodies were

incubated in serum at 37°C for different time intervals, followed by HPLC analysis to evaluate their stability.

Cell culture

Wild-type (Tn-) murine lung cancer cell line LL/2 (ATCC), and LL/2 cells expressing the Tn antigen (Tn+) (da Costa et al., 2021), were grown in RPMI-1640 medium (Capricorn Scientific) supplemented with 10% Fetal Bovine Serum (FBS, Capricorn Scientific), 2 mM L-Glutamine, 100 U/mL penicillin and 100 µg/mL Streptomycin (Capricorn Scientific). All cultures were incubated at 37 °C with 5% CO₂ and a 95% humidity atmosphere.

Membrane-bound and cell internalization

Membrane-bound and cell internalization assay was performed by seeding 0.5×10^6 Tn- or Tn + cells with culture medium in 24 well plates and allowed to grow overnight. After washing once with culture medium, cells were incubated with ~4 nM of ChiTn and/or IgG radioconjugated with ^{99m}Tc and/or ¹³¹I for 1, 2, 3, 4 (quadruplicates) and 24 h (octuplicate) at 37 °C. Then, the reaction medium was aspirated and cells were washed twice with 500 µL cold Phosphate-buffered saline (PBS). Cells were washed with cold acid buffer solution (0.2 M pH 2 glycine buffer) for 5 min to remove membrane-bound radioconjugated antibodies. The remaining internalized radioconjugated antibodies were obtained by lysis with 1 M NaOH for 5 min. Membrane-bound and internalized radioactivities were measured, and the results were analyzed, according to Radioactivity measurements and Statistical analysis sections.

Animals and tumor induction

C57BL/6 female mice were purchased from URBE Laboratories (Uruguay). Mouse handling, care, and experiments were in accordance with ethical principles adopted by National Committee on Animal Research (CNEA, Uruguay) (protocol approved by the Commission of Ethics in the Use of Animals, Facultad de Ciencias (CEUA) number 240011-001327-18). Tn- or Tn + LL/2 cells (2×10^5 /100 µL) were inoculated on the flank region of each mouse via subcutaneous (s.c.) or intradermal (i.d.) injection (5 mice/group). The animals were followed daily for at least 1 month, evaluating tumor growth. All procedures were confirmed to comply with ARRIVE guidelines.

Losartan treatment

Losartan pills (50 mg/pill) (Losartan potassium) were ground using a mortar and pestle, and dissolved in PBS to obtain a concentration of 2.5 mg/mL. The solutions were then filtered and stored in a sterile container. Animals were treated daily with an intraperitoneal (i.p.) injection of Losartan (20 mg/kg) or saline (control) for 9 days (Diop-Frimpong et al., 2011; Chauhan et al., 2013; Zhao et al., 2019).

Biodistribution studies

When tumors reached 500–1000 cm³ in size (15–20 days), mice from the same cohort received 0.74-3 MBq of ChiTn-HYNIC-^{99m}Tc or IgG-HYNIC-^{99m}Tc (1–4 µg, in 100 µL PBS), and/or approximately 185 kBq

of ChiTn-¹³¹I or IgG-¹³¹I (1 µg, in 100 µL PBS) via the tail vein. After 4, 24, and 48 h, the animals were euthanized with anesthetic drugs (xylazine-100 mg/Kg and ketamin-300 mg/Kg). Blood, urine, and feces were collected, tumor and selected organs were excised, rinsed of residual blood, weighed and their radioactivity was measured according to the Radioactivity measurements section. Results were expressed as percent injected dose (% ID) and per gram of tissue (% ID/g).

Radioactivity measurements

Gamma-ray measurements were acquired using a high-purity germanium detector (HPGe) (Canberra) and appropriate low-background shielding. The HPGe has the following features: 20% counting efficiency (at 1332 keV) and FWHM resolution < 0.85 keV (at 122 keV), enabling simultaneous *in vitro* and/or biodistribution measurements of multiple gamma-emitting radionuclide (Knight et al., 2019; Tassano et al., 2021). Results are reported for ^{99m}Tc (140.5 keV, 89%) lower limit of detection (LLD) 110 Bq, and ¹³¹I (364.5 keV, 81.7%) LLD 1.0 kBq for 30-second measurements.

Statistical analysis

To evaluate the statistical significance of differences in medians, we used the Mann-Whitney U test (MW) with Bonferroni correction. The following annotation was used for statistical significance, ns: $p < = 1e^{+00}$; *: $1e^{-02} < p < = 5e^{-02}$; **: $1e^{-03} < p < = 1e^{-02}$; ***: $1e^{-04} < p < = 1e^{-03}$; ****: $p < = 1e^{-04}$, also, a 95% confidence interval (CI) was applied. We performed all statistical analyses and data visualizations using multiple packages within Spyder v. 4.1.5 (Raybaut, 2009), an integrated development environment (IDE) for scientific programming in Python v. 3.8.5 (Python Software Foundation). The packages utilized include Pandas (McKinney, W., 2010) for data manipulation, Matplotlib (Hunter, J. D., 2007) for data visualization, NumPy (Harris et al., 2020) for numerical computations, Seaborn (Waskom et al., 2021) for advanced data visualization, and Statannotations (Charlier et al., 2022) for statistical annotations.

Results

Radiolabeling and in vitro quality controls

Both ¹³¹I and ^{99m}Tc radiolabeled ChiTn or IgG antibodies were purified and their chemical identity was determined by SEC, HPLC, and ITLC. SEC analysis showed a retention volume of the radiolabeled antibodies between 3–4 mL, while free ^{99m}Tc and free ¹³¹I showed a retention volume between 8–9 mL. HPLC profile showed retention times of 8.5, 8.9, and 9.0 min for ChiTn-HYNIC-^{99m}Tc, ChiTn-¹³¹I, and unlabeled ChiTn respectively (Fig. 1). Radiochemical purity exceeded 92% in all the experiments. The analysis conducted by ITLC demonstrated that within the residual 8%, nearly two-thirds were attributed to ^{99m}TcO₂.H₂O, while the remaining one-third was associated with ^{99m}Tc-tricine. The radiochemical stability exhibited a gradual decrease over time, with an average of 89% (SD 2.1) and 90% (SD 2.08) of antibodies retaining their radiolabeling with ^{99m}Tc and ¹³¹I, respectively, after a 48 h incubation period in

serum at 37 °C (Fig. 1, lower right). Similar results of radiochemical purity and stability were obtained for IgG-HYNIC-^{99m}Tc (data not shown).

Membrane-bound and cell internalization

Results for the membrane-bound, internalization, and uptake ratio between Tn + and Tn- LL/2 cells for radioconjugated ChiTn and/or IgG are shown in Fig. 2, and data are available at <https://zenodo.org/record/8110446>. A gradual, time-dependent increase in both membrane-bound and intracellular activities was observed for ChiTn-HYNIC-^{99m}Tc during the 24 h experiment at 37°C (Fig. 2A). This increase was found to be significantly higher in Tn + cells compared to Tn- cells ($p < = 1e-04$ at 24 h). Similarly, when IgG-HYNIC-^{99m}Tc and ChiTn-¹³¹I were co-incubated, a similar trend of gradual increase was observed for ChiTn-¹³¹I, with significantly higher activities observed in Tn + cells ($1e-03 < p < = 1e-02$ at 24 h). However, no specific trend or significant differences were observed between Tn + and Tn- cells when using IgG-HYNIC-^{99m}Tc (Fig. 2B). The total cell-associated uptake of ChiTn-HYNIC-^{99m}Tc was approximately 100% higher in Tn + cells compared to Tn- cells, while for ChiTn-¹³¹I, the difference was approximately 50% (Fig. 2C at 24 h). In contrast, no significant difference favoring Tn + cells was observed for IgG-HYNIC-^{99m}Tc (Fig. 2C).

Biodistribution studies

The results of the biodistribution of ChiTn-HYNIC-^{99m}Tc in female C57BL/6 inoculated s.c. or i.d. with Tn- or Tn + LL/2 cells obtained at 4, 24, 48 h post-injection, are shown in Fig. 3 and Sup. Figure 1, and data are available at <https://zenodo.org/record/8110446>. An increase in Tn + tumor uptake occurred between 4 h ($4.4\% \pm 1.6$ ID/g) and 24 h ($10.5\% \pm 2.3$ ID/g) post-injection, remaining stable at 48 h ($11.3\% \pm 2.5$ ID/g). No significant differences in the uptake were found between Tn- and Tn + or between s.c. or i.d. tumors. Furthermore, there were no significant differences between Tn- and Tn + or between s.c. or i.d. tumors concerning the ratios of tumor-to-blood (T/B) and tumor-to-muscle (T/M). The remaining organs showed a typical antibody biodistribution profile, with liver uptake and hepatobiliary elimination (Sup. Figure 1).

The biodistribution of double-labeled ChiTn with ^{99m}Tc and ¹³¹I at 48h post-injection (Fig. 4 above) resulted in a profile with higher values for ^{99m}Tc in the liver, spleen, kidneys and a tendency to show higher values in Tn- and Tn + tumors, although this was not significant. The ¹³¹I shows a high preference for the thyroid and is also significantly higher in the stomach. No significant differences were found in the T/B and T/M ratios. Also, the biodistribution of the co-injection of IgG-HYNIC-^{99m}Tc and ChiTn-¹³¹I was performed at 48 h (Fig. 4 below). Most of the organs showed a higher %ID/g of IgG-HYNIC-^{99m}Tc compared to ChiTn-¹³¹I, even in the Tn- tumor, but not in the Tn+. Increased uptake was also found in the thyroid by ChiTn-¹³¹I. No significant differences were found in the T/B and T/M ratios, for both biodistributions. All values, except for thyroid, are comparable to Fig. 3 and Sup. Figure 1. Data available at <https://zenodo.org/record/8110446>.

Finally, the biodistribution of ChiTn-HYNIC-^{99m}Tc and IgG-HYNIC-^{99m}Tc at 48 h in mice pre-treated with Losartan is shown (Fig. 5), data available at <https://zenodo.org/record/8110446>. Although the profile was similar to Fig. 3 and 4, interestingly a higher uptake was observed in Tn+ than in Tn- tumors for ChiTn-HYNIC-^{99m}Tc. Also, higher T/B and T/M ratios were observed between Tn+ and Tn- tumors for ChiTn-HYNIC-^{99m}Tc. No significant differences between Tn+ and Tn- tumors were observed for IgG-HYNIC-^{99m}Tc. The average results and their standard deviation are summarized in Table 1.

Table 1. Total 48 h biodistribution results for Tn+ and Tn- tumors, including %ID/g averages, standard deviations, tumor-to-blood (T/B), and tumor-to-muscle (T/M) ratios.

Molecule	Pre-treatment	Tn- %ID/g (SD)	Tn+ %ID/g (SD)	Tn- T/B (SD)	Tn+ T/B (SD)	Tn- T/M (SD)	Tn+ T/M (SD)
ChiTn-HYNIC-99mTc	Untreated	10.3 (± 3.5)	11.3 (± 2.5)	0.5 (± 0.2)	0.8 (± 0.5)	5.2 (± 2.9)	7.7 (± 3.3)
IgG-HYNIC-99mTc	Untreated	14.5 (± 0.7)	14.7 (± 2.6)	0.8 (± 0.3)	0.6 (± 0.1)	5.7 (± 0.8)	8.4 (± 3.6)
ChiTn-131I	Untreated	5.2 (± 1.1)	9.1 (± 2.2)	0.5 (± 0.3)	0.5 (± 0.2)	2.7 (± 0.9)	5.3 (± 2.6)
ChiTn-HYNIC-99mTc	Losartan	7.9 (± 1.2)	14.9 (± 2.1)	0.6 (± 0.1)	1.2 (± 0.2)	4.3 (± 0.8)	10.4 (± 3.3)
IgG-HYNIC-99mTc	Losartan	10.9 (± 2.5)	8.4 (± 1.9)	0.5 (± 0.2)	0.4 (± 0.1)	4.6 (± 1.9)	3.4 (± 1.6)

Discussion

Effective drug delivery to tumors is often hindered by several barriers, such as physical barriers, low oxygen levels, and acidic pH, impeding the penetration of anticancer agents (Curti, 1993; Sriraman et al., 2014). Physical barriers include the interstitial transport of antibodies in normal and neoplastic tissues (Curti, 1993, Libuti et al., 2018). Such barriers could explain why some drugs, effective *in vitro*, fail to work *in vivo* (Jain, 1994; Anchordoquy et al., 2017). To address this, we investigated the potential of Losartan to enhance the delivery of the ChiTn antibody to Tn + tumors by reducing solid stress (Diop-Frimpong et al., 2011, Chauhan et al., 2013, Zhao et al., 2019). We evaluated the radiolabeled mAb ChiTn intending to use it as a tracer, but also as a potential cancer theranostic agent.

Our experimental findings demonstrate that the radiochemical purity of both ^{99m}Tc and ¹³¹I radiolabeled antibodies remained consistently above 92% even after a 48 h incubation period in serum at 37 °C (Fig. 1). These results align with previous studies that reported similar levels of radiochemical purity and stability over time using the same antibody labeling methodology with ^{99m}Tc (Camacho et al., 2017; Perroni et al., 2021) and ¹³¹I (Vinod et al., 2021).

Different binding and internalization capacities of the ChiTn mAb to tumor cell lines expressing the Tn-antigen have been observed (Hubert et al., 2011; Sedlik et al., 2016', Castro et al., 2021). Additionally, it is rapidly internalized by Tn + tumor cells and primarily localizes in early endosomes (Hubert et al., 2011; Sedlik et al., 2016). Our results show that membrane-bound and internalization of the labeled antibody in Tn + and Tn- LL/2 cells exhibit slower kinetics than the unlabeled antibody, but are similar to those of

other radiolabeled antibodies (Kuo et al., 2018; Camacho et al., 2014). The ^{99m}Tc labeling process involves the reaction of HYNIC with, for example, the ϵ -amino group of antibody lysines (Meszaros et al., 2010; Garcia et al., 2016). Similarly, for the chemical oxidation process used in ^{131}I labeling, sodium iodide is converted into a reactive form that can be incorporated into the tyrosyl groups of the antibody (Gupta et al., 2014; Feng et al., 2022). Therefore, modification by radioactive labeling can alter the physical and chemical properties of the antibody, which can affect its interaction with cells (Tolmachev et al., 2014).

ChiTn-HYNIC- ^{99m}Tc showed persistent membrane binding after 24 h, favoring Tn + cells significantly (Fig. 2A). Notable Tn + internalization was observed after 4 h (Fig. 2A). ChiTn- ^{131}I yielded similar results unlike the control IgG-HYNIC- ^{99m}Tc , which showed minimal binding and internalization with no significant Tn + and Tn- differences (Fig. 2B). Figure 2C illustrates the disparities in Tn+/Tn- ratios.

Although intermediate affinities of radiolabeled antibodies may hinder binding and internalization, studies by Rudnick et al. have shown that low-affinity mAbs can penetrate solid tumors more efficiently (Rudnick et al., 2011). To investigate the uptake and retention ability of radiolabeled ChiTn and IgG in Tn + and Tn- tumors *in vivo*, we conducted various biodistribution studies.

The biodistribution results of ChiTn-HYNIC- ^{99m}Tc indicated a typical distribution pattern for ^{99m}Tc radiolabeled antibodies through HYNIC, as reported by Camacho et al. (2014). The radiotracer exhibited slow clearance in the bloodstream, liver, heart, and lungs, and sustained tumor uptake up to 48 h ($11.3 \pm 2.5\% \text{ID/g}$), with no significant differences between Tn + and Tn- tumors or T/B and T/M ratios (Fig. 2, 3, and Sup. Figure 1). Similar results were seen for i.d. and s.c. injections of LL/2 Tn + and Tn- cells in mice.

To assess the impact of the radioactive labeling method on biodistribution (Williams, 2014), we performed dual-labeling of the ChiTn antibody with ^{99m}Tc and ^{131}I . This enabled simultaneous measurement of biodistribution using gamma spectrometry (Tassano et al., 2021), thereby minimizing inter-mouse, inter-measurement, and handling variability (Knight et al. 2019). Double-labeled ChiTn exhibited higher values for ^{99m}Tc in the liver, spleen, and kidneys, with a slight tendency for higher values in both Tn- and Tn + tumors (Fig. 4 above), but this was not significant. The ^{131}I exhibited a high affinity for the thyroid and was also significantly higher in the stomach. The T/B and T/M ratios did not show any significant differences.

When radioiodinated antibodies are taken up by cells, they are quickly broken down in lysosomes, resulting in the release of monoiodotyrosine into the extracellular space. This metabolite is further broken down by deiodination enzymes, which release free radioiodide into the bloodstream (Press et al., 1996). The radioiodide is then taken up by any tissues expressing the sodium-iodide (Na^+/I^-) symporter, which is present in the thyroid gland and stomach. The lysosomal degradation of radioiodinated antibodies leads to the rapid clearance of radioiodine from all tissues, except those that metabolize or process iodine (Vivier et al., 2018). This occurrence leads to diminished activity concentrations within the tumor tissue in comparison to residualizing radiolabels that employ the radiometal ^{99m}Tc (Deyev et al., 2020).

The accumulation of the antibody within tumors ideally would solely rely on the specific target antigen. However, challenges arise when non-specific factors contribute to overall tumor uptake. One example is the enhanced permeability and retention (EPR) effect, which occurs due to rapid and irregular angiogenesis, resulting in antibodies passively extravasating into the tumor tissue through the leaky vasculature (Henweeer et al., 2011; Fang et al., 2011). These non-specific contributions to tumor uptake can vary significantly between tumor models, within a single tumor (intra-tumoral heterogeneity), or as a result of different responses to treatment (inter-tumoral heterogeneity). Consequently, the sensitivity of these techniques may be reduced, increasing the likelihood of false discoveries (Börjesson et al., 2006).

We conducted an additional experiment to assess non-specific uptake by comparing the biodistribution of Tn-specific ChiTn-¹³¹I with that of non-specific IgG-HYNIC-^{99m}Tc. Most of the organs showed a higher % ID/g of IgG-HYNIC-^{99m}Tc compared to ChiTn-¹³¹I (Fig. 4 below). This is expected since the radioactive label with ¹³¹I tends to be more unstable *in vivo*, leading to increased uptake in the thyroid and stomach, as well as greater clearance from organs, as previously discussed. Nevertheless, the Tn + tumor demonstrated a comparable uptake of ChiTn-¹³¹I to that of IgG-HYNIC-^{99m}Tc, while a reduced uptake was observed in Tn- tumors. Once again, no distinct advantage in uptake was noted for the Tn-specific ChiTn as compared to the non-specific IgG. This observation is further corroborated by the similarities in the tumor-to-blood (T/B) and tumor-to-muscle (T/M) ratios (Fig. 4 below).

The presence of solid stress may be a contributing factor hindering the efficient delivery of antibodies to tumors, particularly in highly vascularized tumors such as LL/2 Tn+. These tumors produce higher levels of VEGF compared to LL/2 wild type (Tn-), as demonstrated by da Costa et al. (2021). VEGF is recognized as a key factor in angiogenesis, capable of inducing ECM synthesis and promoting the angio-fibrotic switch in fibrosis, as documented by Larsson-Callerfelt et al. (2017), Kuiper et al. (2008), and Zhang et al. (2019). The fibrotic ECM significantly contributes to elevated solid stress within tumors (Jain et al., 2014).

To assess this phenomenon, biodistribution studies were conducted after pretreatment with Losartan, a compound known to alleviate solid stress in fibrotic tumors (Diop-Frimpong et al., 2011; Chauhan et al., 2013). Previous research has indicated that Losartan treatment does not alter VEGF levels or microvessel density. However, it has been shown to significantly enhance the percentage of perfused blood vessels (Zhao et al., 2019).

The % ID/g values indicate that the biodistribution profiles of normal tissues in the Losartan pre-treated mice (Fig. 5) were comparable to those of the untreated counterparts at 48 h post-injection for both IgG-HYNIC-^{99m}Tc and ChiTn-HYNIC-^{99m}Tc, which aligns with the findings of Chauhan et al. (2013) where Losartan treatment does not affect accumulation in normal tissues. However, a slightly higher uptake in the kidneys and elimination through urine and feces were observed for ChiTn-HYNIC-^{99m}Tc (Fig. 5). Additionally, ChiTn-HYNIC-^{99m}Tc demonstrated a higher blood clearance compared to IgG-HYNIC-^{99m}Tc, as evident in Fig. 5, consistent with the outcomes of the previous biodistribution studies where ChiTn-HYNIC-^{99m}Tc values ranged from 15 to 20% ID/g and IgG-HYNIC-^{99m}Tc values ranged from 22 to 30% ID/g at 48 h in bloodstream (Fig. 3, 4, and 5).

In mice pre-treated with Losartan, a significantly higher uptake of ChiTn-HYNIC-^{99m}Tc was observed in Tn + tumors (%ID/g 14.9 ± 2.1) compared to Tn- tumors (%ID/g 7.9 ± 1.2) ($p \leq 0.05$), as indicated in Table 1 and Fig. 5. However, there was no significant change in the uptake of IgG-HYNIC-^{99m}Tc in either tumor type. These findings are further supported by the T/B and T/M ratios (Table 1 and Fig. 5). ChiTn-HYNIC-^{99m}Tc demonstrated significantly higher ratios in favor of Tn + over Tn- tumors ($p \leq 0.01$ and $p \leq 0.05$, respectively), while IgG-HYNIC-^{99m}Tc did not show the same pattern. Specifically, the T/B ratio in Tn + tumors increased from 0.8 ± 0.5 in untreated mice to 1.2 ± 0.2 in mice pre-treated with Losartan for ChiTn-HYNIC-^{99m}Tc. The T/M ratio also exhibited a moderate increase from 7.7 ± 3.3 to 10.4 ± 3.3 .

These values indicate a substantial increase in Tn + uptake compared to Tn- in mice pre-treated with Losartan, with an average of 88% higher uptake in Tn + tumors. Additionally, there was a significant enhancement in the T/B ratio, with a 50% increase. Similarly, the T/M ratio exhibited a 35% increase in Tn + tumors. All of these values closely align with the findings reported by Chauhan et al. (2013), where Losartan treatment resulted in a 74% increase in the accumulation of the small-molecule chemotherapeutic 5-FU in AK4.4 pancreatic tumors.

The findings indicate that LL/2 Tn + tumors exhibit elevated solid stress compared to their wild-type (Tn-) counterparts. As a result, Losartan is expected to be more effective in alleviating this stress specifically in Tn + tumors. Additionally, the radiolabeled ChiTn mAb demonstrates enhanced penetration into this tumor type, allowing for increased interaction with the Tn antigen. In contrast, nonspecific IgG lacks the capability to undergo specific binding and subsequent internalization into tumor cells, leading to a lack of this effect. Its uptake primarily occurs through nonspecific binding or due to its higher concentration in the bloodstream.

In conclusion, our study investigated the use of radiolabeled mouse/human chimeric anti-Tn antibody (ChiTn) as a tracer and cancer theranostic agent in combination with Losartan in mice with Tn-expressing lung tumors. We found that radiolabeled ChiTn exhibited greater binding and internalization in Tn + tumor cells compared to Tn- cells. Furthermore, Losartan treatment improved the *in vivo* uptake of radiolabeled ChiTn in Tn + tumors, suggesting enhanced tumor targeting. However, there were no significant differences in biodistribution between Tn + and Tn- tumors for radiolabeled IgG unspecific control molecule. The study provides insights into the potential use of radiolabeled ChiTn in combination with Losartan for improved delivery and targeting of Tn + tumors, which may have clinical implications for the treatment of epithelial cancers expressing the Tn-antigen. Further studies are warranted to explore the theranostic efficacy of this approach and optimize the radiolabeling and targeting strategies.

Declarations

Acknowledgements

This work is part of the Master's and Doctoral Program in Medical Sciences (Proinbio) from the Facultad de Medicina at the Universidad de la Republica, Uruguay, where MSc. Marcos Tassano is pursuing his

doctorate in medical science. We would like to extend special thanks to MD-PhD Roger Chammas, Professor of Oncology and Deputy Dean at the Faculty of Medicine of the University of São Paulo and the Cancer Institute of the State of São Paulo, for his insightful advice on the use of Losartan for tumor delivery.

Author contributions

M.T., X.C., C.P., M.C., M.F.G., M. F., J.P.G. and P.C. participated in the antibody radiolabeling and *in vitro/in vivo* studies in both models. T.F., V.D.C., and E.O., developed cell lines, tumor models and the ChiTn antibody. M.T. drafted the manuscript. All authors participated in the editing and review of the manuscript.

Data availability statement

Comprehensive datasets for *in vitro* and biodistribution assays can be accessed via this link: <https://zenodo.org/record/8110446>.

Additional Information

The authors declare no competing interests.

References

1. Anchordoquy TJ., Barenholz Y, Boraschi D, Chorny M, Decuzzi P, Dobrovolskaia MA, Farhangrazi S, Farrell D, Gabizon A, Ghandehari H, Godin B, La-Beck NM, Ljubimova J, Moghimi SM, Pagliaro L, Park JH, Peer D, Ruoslahti E, Serkova NJ, Simberg D. Mechanisms and Barriers in Cancer Nanomedicine: Addressing Challenges, Looking for Solutions. *ACS Nano* 2017 11 (1), 12–18 DOI: 10.1021/acsnano.6b08244.
2. Ando H, Matsushita T, Wakitani M, Sato T, Kodama-Nishida S, Shibata K, Shitara K, Ohta S. Mouse-human chimeric anti-Tn IgG1 induced anti-tumor activity against Jurkat cells *in vitro* and *in vivo*. *Biol Pharm Bull* 2008; 31:1739–44; PMID:18758069; <http://dx.doi.org/10.1248/bpb.31.1739>
3. Audicio P, Castellano G., Tassano M., Rezzano MR., Fernandez M., Riva E., Robles A., Cabral P., Balter H., Oliver P. [177Lu]DOTA-anti-CD20: Labeling and pre-clinical studies, *Applied Radiation and Isotopes*, Volume 69, Issue 7, 2011, Pages 924–928, ISSN 0969–8043, <https://doi.org/10.1016/j.apradiso.2011.01.026>.
4. Börjesson PKE, Jauw YWS, Boellaard R, de Bree R, Comans EFI, Roos JC, et al. Performance of immuno-positron emission tomography with zirconium-89-labeled chimeric monoclonal antibody U36 in the detection of lymph node metastases in head and neck cancer patients. *Clin Cancer Res* 2006;12:2133.
5. Buss, N. A., Henderson, S. J., McFarlane, M., Shenton, J. M. & de Haan, L. Monoclonal antibody therapeutics: history and future. *Curr. Opin. Pharmacol.* 12, 615–622 (2012).

6. Camacho X, García MF, Calzada V, Fernandez M, Alonso O, Gambini JP, Barbosa de Aguiar R, Longo Machado CM, Chammas R, Porcal W, Cabral P. (2014). 99mTc-Labeled Bevacizumab via HYNIC for Imaging of Melanoma. *Journal of Analytical Oncology*, 3(1), 53–64. <https://doi.org/10.6000/1927-7229.2014.03.01.9>
7. Camacho X, Longo Machado C, García MF, Gambini JP, Banchemo A, Fernández M, Oddone N, Bertolini Zanatta D, Rosal C, Buchpiguel CA, Chammas R, Riva E, Cabral P. Technetium-99m- or Cy7-Labeled Rituximab as an Imaging Agent for Non-Hodgkin Lymphoma. *Oncology* 3 April 2017; 92 (4): 229–242. <https://doi.org/10.1159/000452419>.
8. Castro A, Berois N, Malanga A, Ortega C, Oppezzo P, Pristch O, Mombrú AW, Osinaga E, Pardo H. Docetaxel in chitosan-based nanocapsules conjugated with an anti-Tn antigen mouse/human chimeric antibody as a promising targeting strategy of lung tumors. *Int J Biol Macromol*. 2021 Jul 1;182:806–814. doi: 10.1016/j.ijbiomac.2021.04.054. PMID: 33857513.
9. Chau, C. H., Steeg, P. S. & Figg, W. D. Antibody-drug conjugates for cancer. *Lancet* 394, 793–804 (2019).
10. Chauhan VP, et al. (2013) Angiotensin inhibition enhances drug delivery and potentiates chemotherapy by decompressing tumour blood vessels. *Nat Commun* 4:2516–2527.
11. Charlier F., Weber M., Izak D., Harkin E., Magnus M., Lalli J., Fresnais L., Chan M., Markov N., Amsalem O., Proost S., Krasoulis A., getzze., Repplinger S. (2022). Statannotations (v0.5). Zenodo. <https://doi.org/10.5281/zenodo.7213391>.
12. Curti, BD. Physical barriers to drug delivery in tumors, *Critical Reviews in Oncology/Hematology*, Volume 14, Issue 1, 1993, Pages 29–39, ISSN 1040–8428, [https://doi.org/10.1016/1040-8428\(93\)90004-N](https://doi.org/10.1016/1040-8428(93)90004-N).
13. da Costa V, van Vliet SJ, Carasi P, Frigerio S, García PA, Croci DO, Festari MF, Costa M, Landeira M, Rodríguez-Zraquia SA, Cagnoni AJ, Cutine AM, Rabinovich GA, Osinaga E, Mariño KV, Freire T. The Tn antigen promotes lung tumor growth by fostering immunosuppression and angiogenesis via interaction with Macrophage Galactose-type lectin 2 (MGL2). *Cancer Lett*. 2021 Oct 10;518:72–81. doi: 10.1016/j.canlet.2021.06.012. Epub 2021 Jun 16. PMID: 34144098.
14. Deyev SM., Vorobyeva A., Schulga A., Abouzayed A., Günther T., Garousi J., Konovalova E., Ding H., Gräslund T., Orlova A., Tolmachev V. Effect of a radiolabel biochemical nature on tumor-targeting properties of EpCAM-binding engineered scaffold protein DARPin Ec1, *International Journal of Biological Macromolecules*, Volume 145, 2020, Pages 216–225, ISSN 0141–8130, <https://doi.org/10.1016/j.ijbiomac.2019.12.147>.
15. Diop-Frimpong B, Chauhan VP, Krane S, Boucher Y, Jain RK (2011) Losartan inhibits collagen I synthesis and improves the distribution and efficacy of nanotherapeutics in tumors. *Proc Natl Acad Sci USA* 108:2909–2914.
16. Dovgan, I., Koniev, O., Kolodych, S. & Wagner, A. Antibody-oligonucleotide conjugates as therapeutic, imaging, and detection agents. *Bioconjug. Chem.* 30, 2483–2501 (2019).

17. Duatti A. Review on ^{99m}Tc radiopharmaceuticals with emphasis on new advancements, *Nuclear Medicine and Biology*, Volume 92, 2021, Pages 202–216, ISSN 0969–8051, <https://doi.org/10.1016/j.nucmedbio.2020.05.005>.
18. García MF, Zhang X, Shah M, Newton-Northup J, Cabral P, Cerecetto H, Quinn T. (99m)Tc-bioorthogonal click chemistry reagent for *in vivo* pretargeted imaging. *Bioorg Med Chem*. 2016 Mar 15;24(6):1209–15. doi: 10.1016/j.bmc.2016.01.046. Epub 2016 Jan 29. PMID: 26875936; PMCID: PMC4841469.
19. García, M.F.; Calzada, V.; Camacho, X.; Goicochea, E.; Gambini, J.P.; Quinn, T.P.; Porcal, W.; Cabral, P. Microwave-assisted Synthesis of HYNIC Protected Analogue for ^{99m}Tc Labeled Antibody. *Curr. Radiopharm.*, 2014, 7(2), 84–90.
20. Gupta S, Batra S, Jain M. Antibody labeling with radioiodine and radiometals. *Methods Mol Biol*. 2014;1141:147–57. doi: 10.1007/978-1-4939-0363-4_9. PMID: 24567137; PMCID: PMC4095879.
21. Fang J, Nakamura H, Maeda H. The EPR effect: unique features of tumor blood vessels for drug delivery, factors involved, and limitations and augmentation of the effect. *Adv Drug Deliv Rev* 2011;63:136–51.
22. Feng, Y., Meshaw, R., McDougald, D., Zhou, Z., Zhao, XG., Jannetti, SA., Reiman RE., Phippen E., Marjoram R., Schaal JL., Vaidyanathan G., Zalutsky MR. Evaluation of an ^{131}I -labeled HER2-specific single domain antibody fragment for the radiopharmaceutical therapy of HER2-expressing cancers. *Sci Rep* 12, 3020 (2022). <https://doi.org/10.1038/s41598-022-07006-9>.
23. Fu C, Zhao H, Wang Y, Cai H, Xiao Y, Zeng Y, Chen H. Tumor-associated antigens: Tn antigen, sTn antigen, and T antigen. *HLA*. 2016 Dec;88(6):275–286. doi: 10.1111/tan.12900. Epub 2016 Sep 28. PMID: 27679419.
24. Hafeez, U., Gan, H. K. & Scott, A. M. Monoclonal antibodies as immunomodulatory therapy against cancer and autoimmune diseases. *Curr. Opin. Pharmacol.* 41, 114–121 (2018).
25. Hakomori S. Glycosylation defining cancer malignancy: new wine in an old bottle. *Proc Natl Acad Sci U S A*. 2002; 99:10231–10233.
26. Harris, C. R., Millman, K. J., van der Walt, S.J., Gommers, R., Virtanen, P., Cournapeau, D., Wieser, E., Taylor, J., Berg, S., Smith, N. J., Kern, R., Picus, M., Hoyer, S., H. van Kerkwijk, H., Brett, M., Haldane, A., Fernández del Río, J., Wiebe, M., Peterson, P., Gérard-Marchant, P. Sheppard, K., Reddy, T., Weckesser, W., Abbasi, H., Gohlke C., Oliphant, T.E., 2020. Array programming with NumPy, *Nature*. 585, 357–362. DOI:10.1038/s41586-020-2649-2.
27. Harsini, S., Rezaei, N. (2020). Cancer Imaging with Radiolabeled Monoclonal Antibodies. In: Rezaei, N. (eds) *Cancer Immunology*. Springer, Cham. https://doi.org/10.1007/978-3-030-30845-2_32. Hubert P, Heitzmann A, Viel S, Nicolas A, Sastre-Garau X, Oppezco P, Pritsch O, Osinaga E, Amigorena S. Antibody-dependent cell cytotoxicity synapses form in mice during tumor-specific antibody immunotherapy. *Cancer Res*. 2011 Aug 1;71(15):5134-43. doi: 10.1158/0008-5472.CAN-10-4222. Epub 2011 Jun 22. PMID: 21697279.

28. Heneweer C, Holland JP, Divilov V, Carlin S, Lewis JS. Magnitude of enhanced permeability and retention effect in tumors with different phenotypes: 89Zr-albumin as a model system. *J Nucl Med* 2011;52:625–33.
29. Hunter, J. D., 2007. Matplotlib: A 2D Graphics Environment, *Comput Sci Eng.* 9, 90–95. DOI:10.1109/MCSE.2007.55.
30. Jain, RK. (1994). Barriers to drug delivery in solid tumors. *Scientific American*, 271(1), 58–65.
31. Jain, RK. (2014). Antiangiogenesis strategies revisited: From starving tumors to alleviating hypoxia. *Cancer Cell* 26:605–622.
32. Jain RK, Martin JD, Stylianopoulos T. The Role of Mechanical Forces in Tumor Growth and Therapy. *Annual Review of Biomedical Engineering* 2014 16:1, 321–346.
33. Ju T, Otto VI, Cummings RD. The Tn antigen-structural simplicity and biological complexity. *Angew Chem Int Ed Engl* 2011; 50:1770–91; PMID:21259410; <http://dx.doi.org/10.1002/anie.201002313>
34. Kaplon, H. & Reichert, J. M. Antibodies to watch in 2021. *MAbs* 13, 1860476 (2021).
35. Knight JC, Mosley MJ, Kersemans V, Dias GM, P. Allen D, Smart S, Cornelissen B. Dual-isotope imaging allows *in vivo* immunohistochemistry using radiolabelled antibodies in tumours. *Nuclear Medicine and Biology*, Volume 70, 2019, Pages 14–22, ISSN 0969–8051, <https://doi.org/10.1016/j.nucmedbio.2019.01.010>.
36. Kuiper EJ, Van Nieuwenhoven FA, de Smet MD, van Meurs JC, Tanck MW, et al. The Angio-Fibrotic Switch of VEGF and CTGF in Proliferative Diabetic Retinopathy. (2008) The Angio-Fibrotic Switch of VEGF and CTGF in Proliferative Diabetic Retinopathy. *PLOS ONE* 3(7): e2675. <https://doi.org/10.1371/journal.pone.0002675>.
37. Kuo, WY., Lin, JJ., Hsu, HJ. et al. Noninvasive assessment of characteristics of novel anti-HER2 antibodies by molecular imaging in a human gastric cancer xenograft-bearing mouse model. *Sci Rep* 8, 13735 (2018). <https://doi.org/10.1038/s41598-018-32094-x>.
38. Larsson-Callerfelt AK, Andersson Sjöland A, Hallgren O, Bagher M, Thiman L, Löfdahl CG, Bjermer L, Westergren-Thorsson G. VEGF induces ECM synthesis and fibroblast activity in human lung fibroblasts. *European Respiratory Journal* Sep 2017, 50 (suppl 61) PA1045; DOI: 10.1183/1393003.congress-2017.PA1045.
39. Libutti SK, Tamarkin L, Nilubol N. Targeting the invincible barrier for drug delivery in solid cancers: interstitial fluid pressure. *Oncotarget*. 2018; 9: 35723–35725.
40. Lin M, Paolillo V, Le DB, Macapinlac H, Ravizzini GC. Monoclonal antibody based radiopharmaceuticals for imaging and therapy. *Curr Probl Cancer*. 2021 Oct;45(5):100796. doi: 10.1016/j.currproblcancer.2021.100796. Epub 2021 Oct 4. PMID: 34657748.
41. Liu J, et al. (2012) TGF- β blockade improves the distribution and efficacy of therapeutics in breast carcinoma by normalizing the tumor stroma. *Proc Natl Acad Sci USA* 109:16618–16623.
42. Liu Z, Liu J, Dong X, Hu X, Jiang Y, Li L, Du T, Yang L, Wen T, An G, Feng G. Tn antigen promotes human colorectal cancer metastasis via H-Ras mediated epithelial-mesenchymal transition

- activation. *J Cell Mol Med*. 2019 Mar;23(3):2083–2092. doi: 10.1111/jcmm.14117. Epub 2019 Jan 13. PMID: 30637914; PMCID: PMC6378212.
43. Martineau P, Watier H, Pèlerin A, Turtoi A. Targets for MAbs: innovative approaches for their discovery & validation, LabEx MABImprove 6th antibody industrial symposium, June 25–26, 2018, Montpellier, France. *MAbs*. 2019 Jul;11(5):812–825. doi: 10.1080/19420862.2019.1612691. Epub 2019 May 16. PMID: 31043141; PMCID: PMC6601567.
44. McKinney W., 2010. Data Structures for Statistical Computing in Python, Proceedings of the 9th Python in Science Conference, 51–56.
45. Meszaros LK, Dose A, Biagini SC, Blower PJ. Hydrazinonicotinic acid (HYNIC) – Coordination chemistry and applications in radiopharmaceutical chemistry. *Inorganica Chim Acta* 2010; 363: 1059–69.
46. Nia HT, et al. (2016) Solid stress and elastic energy as measures of tumour mechanopathology. *Nat Biomed Eng* 1:4–29.
47. Osinaga E, Bay S, Tello D, Babino A, Pritsch O, Assemat K, Cantacuzene D, Nakada H, Alzari P. Analysis of the fine specificity of Tn-binding proteins using synthetic glycopeptide epitopes and a biosensor based on surface plasmon resonance spectroscopy. *FEBS Lett*. 2000 Mar 3;469(1):24 – 8. doi: 10.1016/s0014-5793(00)01248-5. PMID: 10708749.
48. Perroni, C., Camacho, X., Tassano, M., Garcia, M., Cabrera, M., Fernandez, J Benech, H Cerecetto, J Gambini, P Cabral. (2021, September). Targeting CD-20 antigen expression in Melanoma with (99m) Technetium-labeled Rituximab. In *EUROPEAN JOURNAL OF NUCLEAR MEDICINE AND MOLECULAR IMAGING* (Vol. 48, No. SUPPL 1, pp. S516-S516). ONE NEW YORK PLAZA, SUITE 4600, NEW YORK, NY, UNITED STATES: SPRINGER.
49. Pinter M, Jain RK. Targeting the renin-angiotensin system to improve cancer treatment: Implications for immunotherapy. *Sci Transl Med*. 2017;9:eaan5616.
50. Press OW; Shan D; Howell-Clark J; Eary J; Appelbaum FR; Matthews D; King DJ; Haines AMR; Hamann P; Hinman L; Shochat D; Bernstein ID, Comparative metabolism and retention of lidine-125, yttrium-90, and indium-111 radioimmunoconjugates by cancer cells. *Cancer Research* 1996, 56 (9), 2123–2129.
51. Python Software Foundation. Python Language Reference, version 2.7. Available at <http://www.python.org>.
52. Raybaut, P., 2009. Spyder-documentation. Available Online at: Pythonhosted.org.
53. Rudnick SI, Lou J, Shaller CC, Tang Y, Klein-Szanto AJ, Weiner LM, Marks JD, Adams GP. Influence of affinity and antigen internalization on the uptake and penetration of Anti-HER2 antibodies in solid tumors. *Cancer Res* 2011; 71:2250–9; PMID:21406401; <http://dx.doi.org/10.1158/0008-5472.CAN-10-2277>.
54. Sedlik C, Heitzmann A, Viel S, Ait Sarkouh R, Batische C, Schmidt F, De La Rochere P, Amzallag N, Osinaga E, Oppezio P, Pritsch O, Sastre-Garau X, Hubert P, Amigorena S, Piaggio E. Effective antitumor therapy based on a novel antibody-drug conjugate targeting the Tn carbohydrate antigen.

- Oncoimmunology. 2016 Apr 22;5(7):e1171434. doi: 10.1080/2162402X.2016.1171434. PMID: 27622021; PMCID: PMC5006918.
55. Scott AM, Wolchok JD, Old LJ. Antibody therapy of cancer. *Nat Rev Cancer* 2012; 12:278 – 87; PMID:22437872; <http://dx.doi.org/10.1038/nrc3236>.
 56. Sriraman SK, Aryasomayajula B, Torchilin VP. Barriers to drug delivery in solid tumors. *Tissue Barriers*. 2014 Jul 22;2:e29528. doi: 10.4161/tisb.29528. PMID: 25068098; PMCID: PMC4106925.
 57. Stylianopoulos T, Munn LL, Jain RK (2018) Reengineering the physical microenvironment of tumors to improve drug delivery and efficacy: From mathematical modeling to bench to bedside. *Trends Cancer* 4:292–319.
 58. Steiner, M. & Neri, D. Antibody-radionuclide conjugates for cancer therapy: historical considerations and new trends. *Clin. Cancer Res.* 17, 6406–6416 (2011).
 59. Tassano, M., Cabrera, M., Camacho, X., Fernandez, M., Garcia, M., Gambini, J. and Cabral, P., 2021, September. Simultaneous Biodistribution Studies of Tc-99m/I-131 Labeled Antibody with HPGe Gamma Spectrometry. In *EUROPEAN JOURNAL OF NUCLEAR MEDICINE AND MOLECULAR IMAGING* (Vol. 48, No. SUPPL 1, pp. S423-S424). ONE NEW YORK PLAZA, SUITE 4600, NEW YORK, NY, UNITED STATES: SPRINGER.
 60. Tolmachev V, Orlova A, Andersson K. Methods for radiolabelling of monoclonal antibodies. *Methods Mol Biol.* 2014;1060:309–30.
 61. Vacchelli E, Eggermont A, Galon J, Sautes-Fridman C, Zitvogel L, Kroemer G, Galluzzi L. Trial watch: monoclonal antibodies in cancer therapy. *Oncoimmunology* 2013; 2:e22789; PMID:23482847; <http://dx.doi.org/10.4161/onci.22789>
 62. Vinod, N., Kim, J.H., Choi, S. et al. Combination of 131I-trastuzumab and lanatoside C enhanced therapeutic efficacy in HER2 positive tumor model. *Sci Rep* 11, 12871 (2021). <https://doi.org/10.1038/s41598-021-92460-0>.
 63. Vivier D, Sharma SK, Zeglis BM. Understanding the *in vivo* fate of radioimmunoconjugates for nuclear imaging. *J Labelled Comp Radiopharm.* 2018 Jul;61(9):672–692. doi: 10.1002/jlcr.3628. Epub 2018 May 14. PMID: 29665104; PMCID: PMC6432633.
 64. Waskom, M. L., (2021). seaborn: statistical data visualization. *Journal of Open Source Software*, 6(60), 3021, <https://doi.org/10.21105/joss.03021>.
 65. Weiner LM, Surana R, Wang S. Monoclonal antibodies: versatile platforms for cancer immunotherapy. *Nat Rev Immunol* 2010; 10:317–27.
 66. Welinder C, Baldetorp B, Borrebaeck C, Fredlund BM, Jansson B. A new murine IgG1 anti-Tn monoclonal antibody with *in vivo* antitumor activity. *Glycobiol* 2011; 21:1097 – 107; PMID:21470982; <http://dx.doi.org/10.1093/glycob/cwr048>
 67. Williams, L. (2014), SU-E-I-14: Comparison of Iodine-Labeled and Indium-Labeled Antibody Biodistributions. *Med. Phys.*, 41: 133–133. <https://doi.org/10.1118/1.4887962>
 68. Zhang, L., Zhao, S., Jiang, H., Zhang, R., Zhang, M., Pan, W., Sun, Z., Wang, D., Li., J. Radioimmunotherapy study of 131I-labeled Atezolizumab in preclinical models of colorectal cancer.

69. Zhang, J.; Chu, M. Differential roles of VEGF: Relevance to tissue fibrosis. *J. Cell. Biochem.* 2019, 120, 10945–10951.
70. Zhao, Y., Cao, J., Melamed, A., Worley, M., Gockley, A., Jones, D., et al. (2019). Losartan Treatment Enhances Chemotherapy Efficacy and Reduces Ascites in Ovarian Cancer Models by Normalizing the Tumor Stroma. *Proc. Natl. Acad. Sci. USA* 116 (6), 2210–2219. doi:10.1073/pnas.1818357116.

Figures

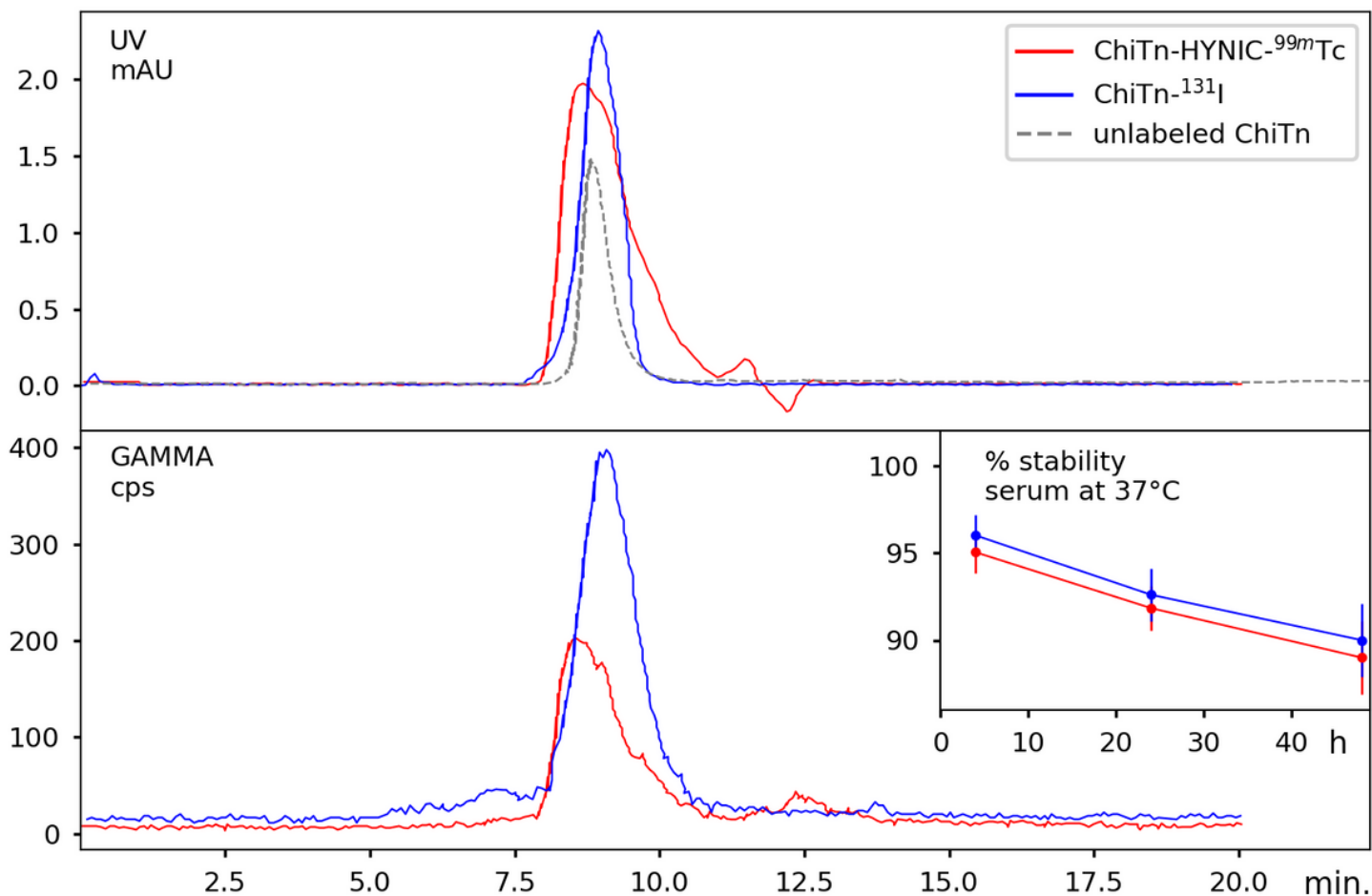


Figure 1

HPLC profile and the *in vitro* radiochemical stability of the radiolabeled ChiTn. The upper panel displays the retention profile of ChiTn when radiolabeled with either ^{99m}Tc (red) or ¹³¹I (blue), as well as unlabeled ChiTn (gray and dashed lines) under UV at a wavelength of 280 nm. The lower panel illustrates the gamma signal of the radiolabeled ChiTn, measured in counts per second. In the bottom right box, the average and standard deviation (SD) of the percentage radiochemical stability of the radiolabeled ChiTn over time in serum at 37°C.

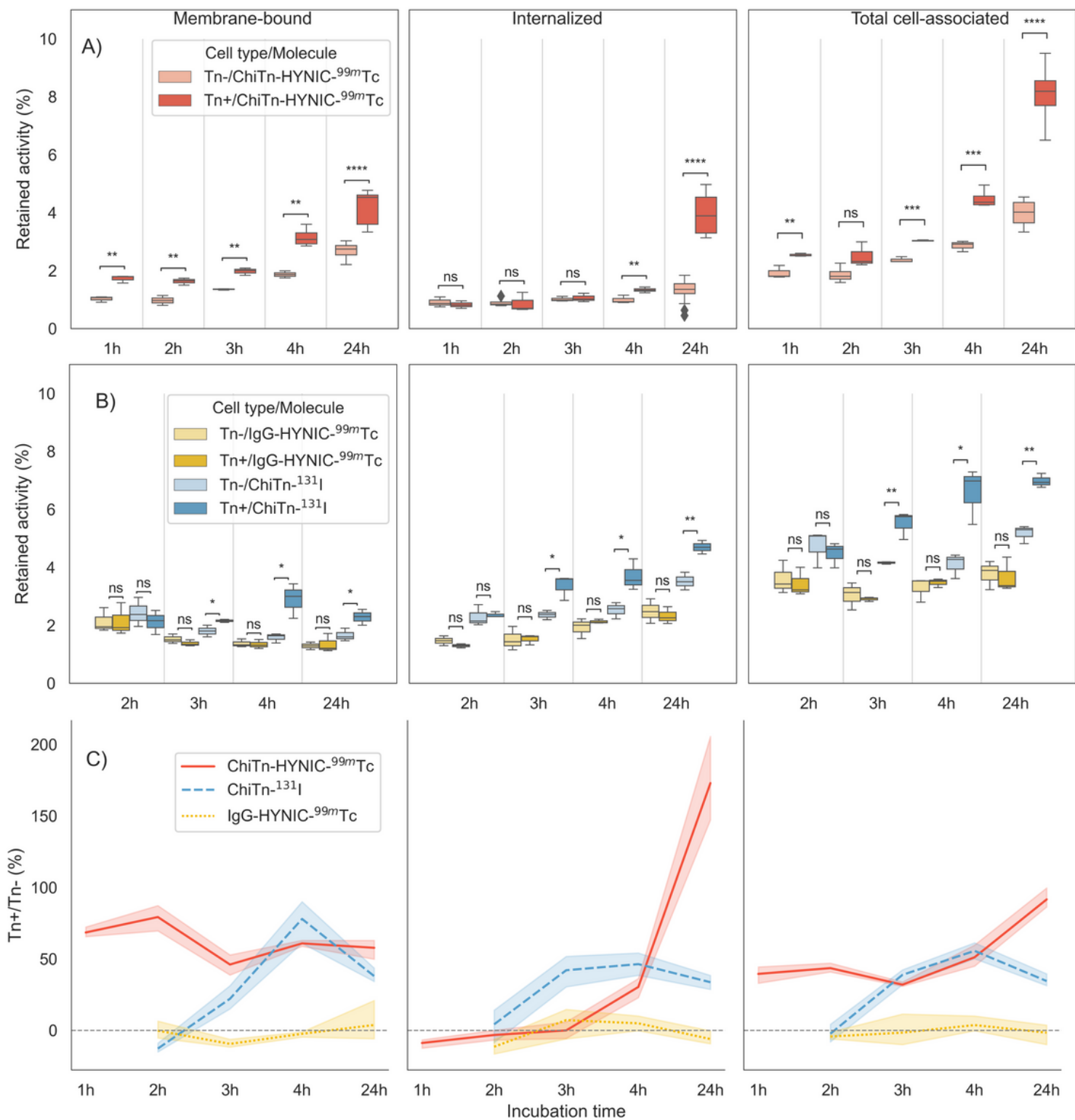


Figure 2

Membrane-bound, internalization, and total cell association of radiolabeled antibodies in LL/2 Tn- or Tn+ cells, measured at different incubation times. The figure includes (A) Boxplot and Mann-Whitney U test (MW) of ChiTn-HYNIC-^{99m}Tc; (B) Boxplot and MW analysis of co-incubated ChiTn-¹³¹I and IgG-HYNIC-^{99m}Tc; and (C) Average and 95% confidence interval (CI) uptake ratio (%) between Tn+ and Tn- cells, for experiments A and B, where positive numbers indicate higher uptake in Tn+ cells.

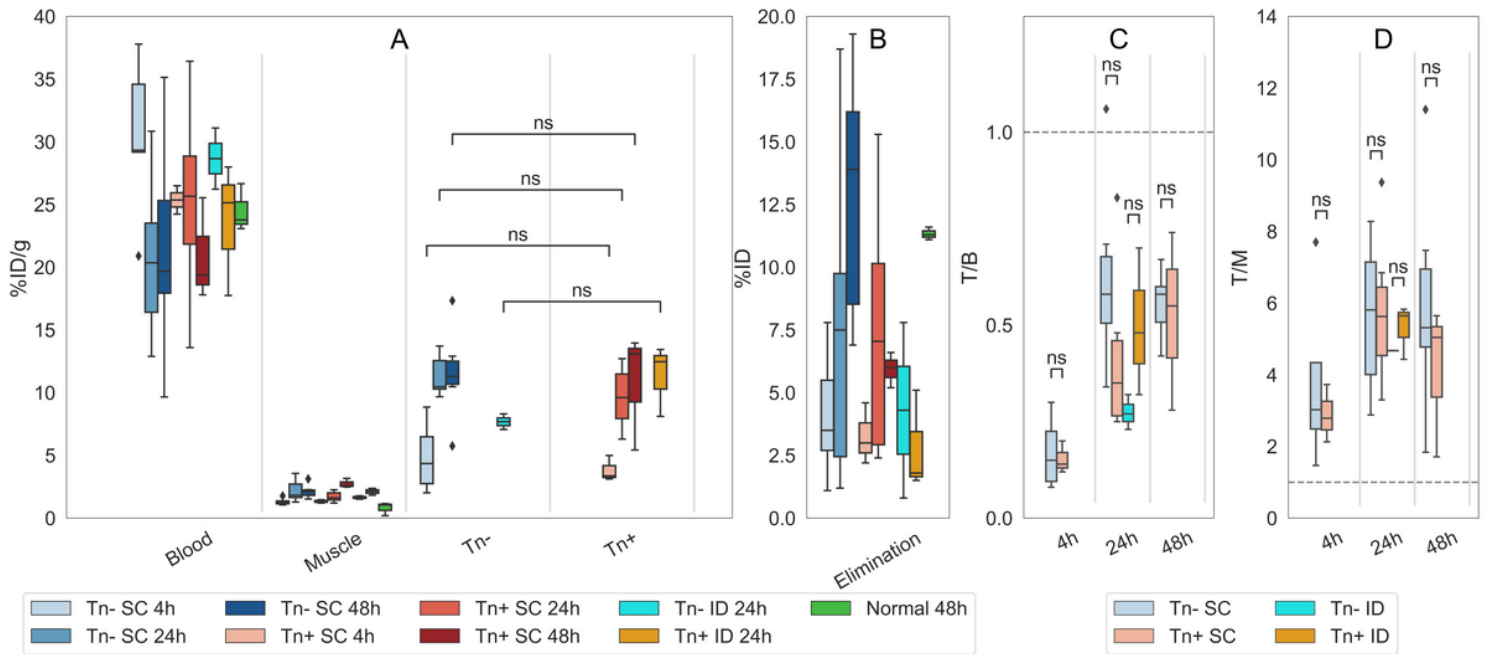


Figure 3

(A) Biodistribution profile of ChiTn-HYNIC-^{99m}Tc in blood, muscle, and Tn- or Tn+ tumors inoculated in mice, by subcutaneous (SC) or intradermal (ID) injection, at 4, 24, and 48 h post-injection. The figure also shows results for non-inoculated (normal) mice. (B) Percent of injected dose (% ID) eliminated via urine and feces. (C and D) Tumor-to-blood (T/B) and tumor-to-muscle (T/M) ratios, respectively.

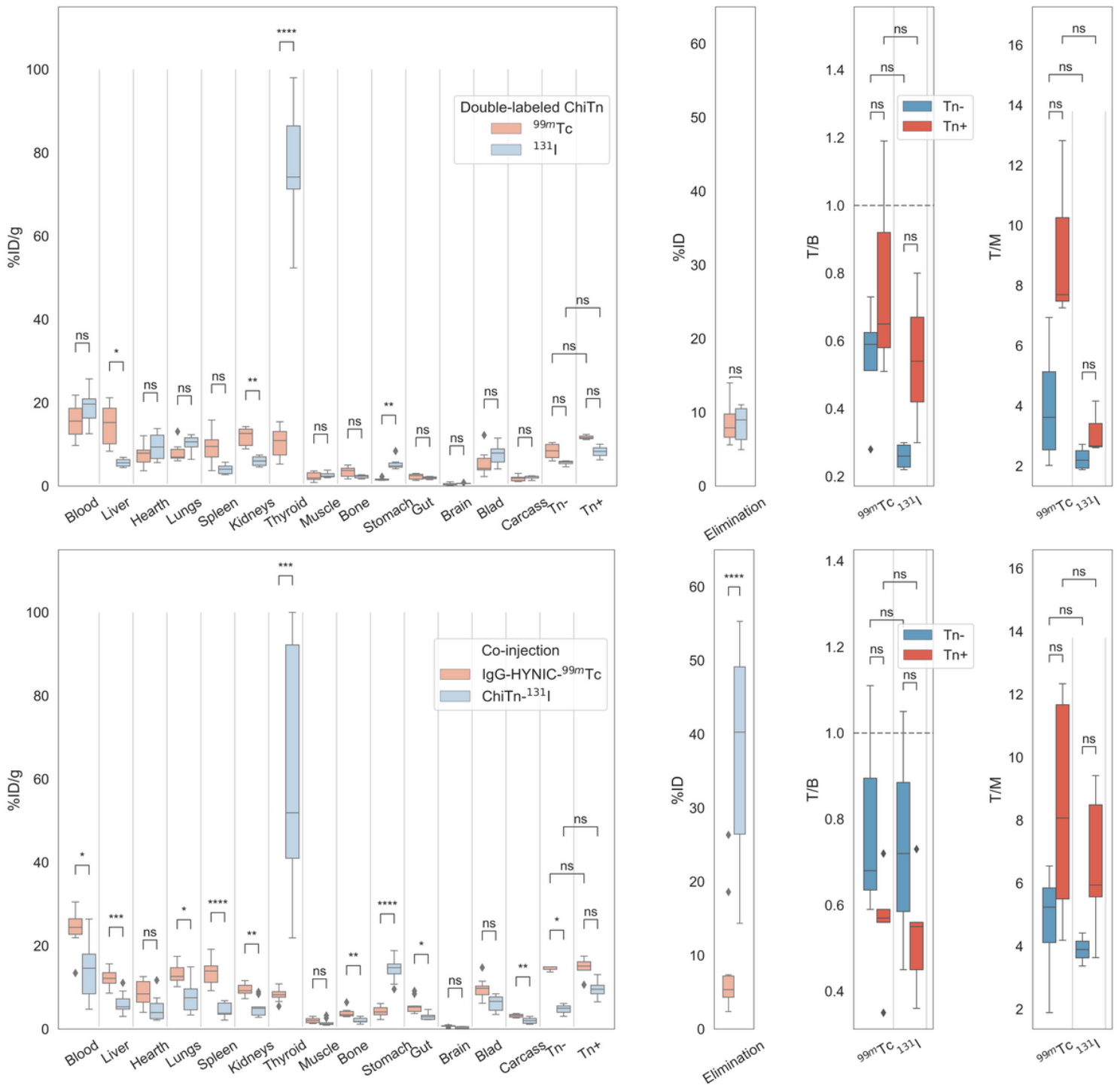


Figure 4

Biodistribution profile of double-labeled ChiTn (^{99m}Tc and ^{131}I) (top panel) and co-injection of IgG-HYNIC- ^{99m}Tc and ChiTn- ^{131}I (bottom panel) at 48 h, in mice with subcutaneous (SC) Tn- or Tn+ tumors. The figure displays elimination (urine + feces), tumor-to-blood (T/B), and tumor-to-muscle (T/M) ratios for each tracer.

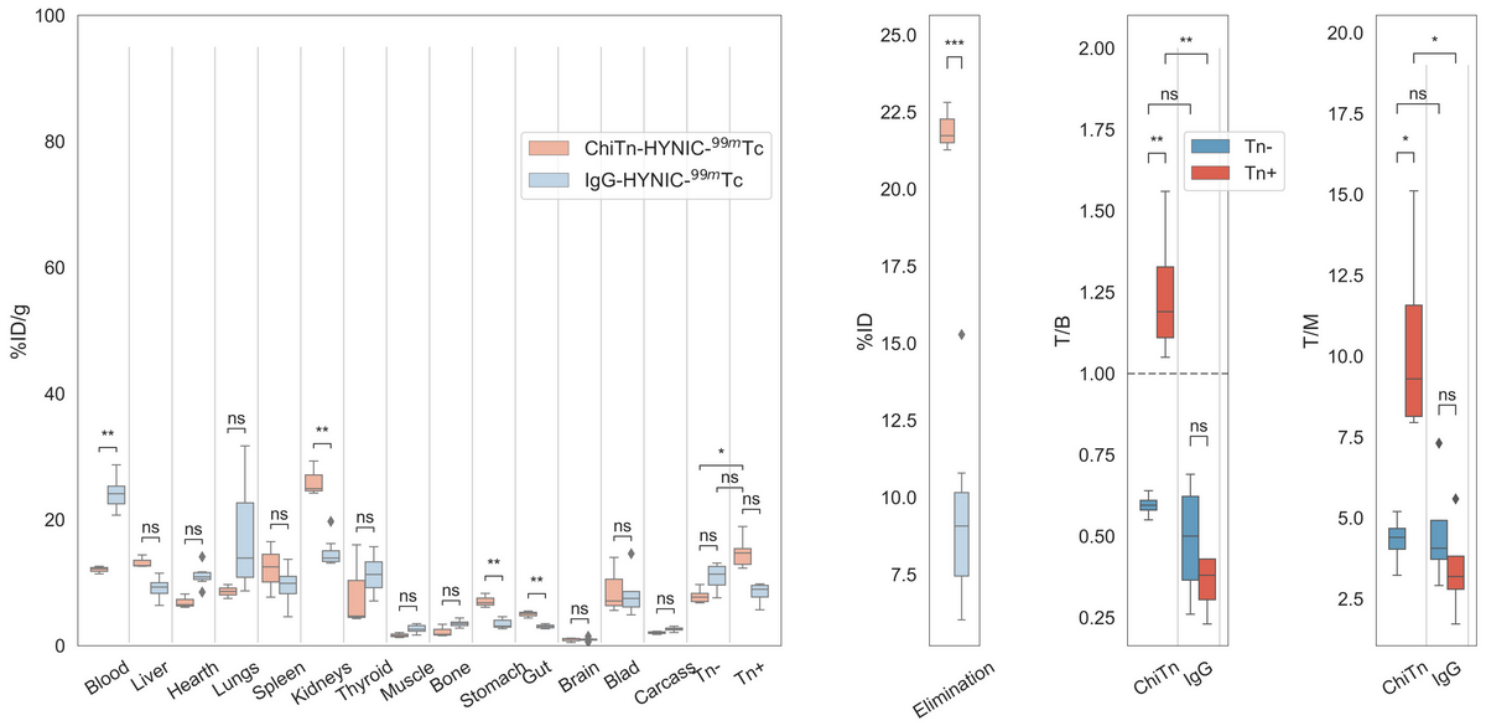


Figure 5

Biodistribution profile of ChiTn-HYNIC-^{99m}Tc and IgG-HYNIC-^{99m}Tc in mice treated with Losartan, at 48 h, with subcutaneous (SC) Tn- or Tn+ tumors. The figure displays elimination (urine + feces), tumor-to-blood (T/B), and tumor-to-muscle (T/M) ratios for both tracers.

Supplementary Files

This is a list of supplementary files associated with this preprint. Click to download.

- [Supplementarymaterial.pdf](#)